

Exchange Interaction in Covalently Bonded Biradical–Monoradical Composite Molecules

Kensuke Maekawa,[†] Daisuke Shiomi,^{*,†,‡,§} Tomoaki Ise,^{†,‡} Kazunobu Sato,[†] and Takeji Takui^{*,†}*Departments of Materials Science and Chemistry, Graduate School of Science, Osaka City University, Sumiyoshi-ku, Osaka 558-8585, Japan, and PRESTO, Japan Science and Technology Agency (JST), 4-1-8 Honcho Kawaguchi, Saitama 332-0012, Japan**Received: August 30, 2004; In Final Form: September 30, 2004*

As a novel molecular designing for genuinely organic molecule-based ferrimagnets, we have proposed a strategy of “single-component ferrimagnetics”. When a π -biradical with an $S = 1$ ground state and a π -monoradical with $S = 1/2$ are united by σ -bonds, the π -conjugation between the biradical and the monoradical moieties should be truncated in the resultant triradical. This gives magnetic degrees of freedom for both $S = 1$ and $1/2$ in the single molecule, serving as a building block for organic molecule-based ferrimagnets under favorable conditions (single-component ferrimagnetics). We have designed and synthesized a triradical, 3-(1'-oxyl-3'-oxido-4',4',5',5'-tetramethylimidazolin-2-yl)benzoic acid 2,4-bis(1''-oxyl-3''-oxido-4'',4'',5'',5''-tetramethylimidazolin-2-yl)phenyl ester (**4**), as a model compound for the novel approach to genuinely organic ferrimagnets. In the triradical **4**, a *m*-phenylene-bis(nitronyl nitroxide) biradical with a triplet ($S = 1$) ground state is united with a phenyl nitronyl nitroxide monoradical ($S = 1/2$) by an ester coupler. Solution-phase ESR spectra from **4** exhibited a complex hyperfine splitting due to ^{14}N and ^1H nuclei. The analysis of the hyperfine structure based on perturbation calculations has revealed that the exchange interaction within the biradical moiety is much larger than those between the biradical and the monoradical moieties and the magnetic degrees of freedom for both $S = 1$ and $1/2$ are retained in **4**. An X-ray crystal structure analysis showed that the triradical molecules are arranged in a one-dimensional molecular chain in the crystal. The magnetic susceptibility in a crystalline solid state is consistent with the crystal structure.

Introduction

The past decades have witnessed a rapid development of molecule-based magnetism.¹ More than 30 ferromagnets have been documented in genuinely organic molecule-based materials¹ after the discovery of the first genuinely organic ferromagnet, *p*-NPNN.² This presents a contrast to the fact that ferrimagnetic spin ordering resulting from an antiparallel coupling of different spin quantum numbers, e.g., $S = 1$ and $1/2$, has never been realized in organic molecular solids. There has been only one report on a model molecular complex of an $S = 1$ biradical and an $S = 1/2$ radical, which exhibits no long-range magnetic ordering.³ Genuinely organic ferrimagnetics has been a challenging and long-standing issue since the first theoretical proposal in 1979.⁴ The first proposal was based on the tendency of the usual organic open-shell molecules to have intermolecular antiferromagnetic interactions in a crystalline solid state. The well-known tendency is seemingly due to the nature of chemical bonding. The authors have presented theoretical consideration in quantum terms on the ferrimagnetic spin alignment in organic molecule-based systems,^{5–7} giving us more evidence-based approaches to organic ferrimagnetism.

As a purposive molecular designing for cocrystallizing distinct molecules with different spin quantum numbers in a solid state, we have proposed a strategy of “single-component ferrimagnetics”:^{8–12} When a π -biradical with a triplet ($S = 1$) ground state and a π -radical with $S = 1/2$ are connected by σ -bonds,

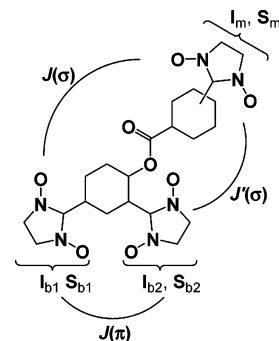


Figure 1. Intramolecular magnetic interactions in the triradicals ($J(\pi)$: the exchange interaction through the π -conjugation within the biradical moiety; $J(\sigma)$, $J'(\sigma)$: the exchange interaction between the biradical and monoradical moieties). I_n and S_n ($n = b1, b2, m$) denote the nuclear and electron spin operators, respectively.

the π -conjugation across the $S = 1$ and $1/2$ moieties is substantially truncated. As a result, additional intramolecular exchange interactions through the σ -bonds in the resultant triradical are expected to be extremely small as compared with the ferromagnetic interaction in the $S = 1$ moiety. The exchange-coupled three-spin system (Figure 1) is described by a Heisenberg spin Hamiltonian

$$H_{\text{ex}} = -2J(\pi)\mathbf{S}_{b1}\cdot\mathbf{S}_{b2} - 2J(\sigma)\mathbf{S}_{b1}\cdot\mathbf{S}_m - 2J'(\sigma)\mathbf{S}_{b2}\cdot\mathbf{S}_m \quad (1)$$

where the two $S = 1/2$ spins, \mathbf{S}_{b1} and \mathbf{S}_{b2} , are coupled by the exchange interaction $J(\pi)$ through the π -conjugation in the biradical moiety and are coupled with another $S = 1/2$ spin, \mathbf{S}_m , in the monoradical moiety by the exchange interactions $J'(\sigma)$ and $J(\sigma)$ through the σ -bonds. In this phenomenological coupling

* Address correspondence to these authors. E-mail: shiomi@sci.osaka-cu.ac.jp, takui@sci.osaka-cu.ac.jp.

[†] Osaka City University.

[‡] PRESTO.

[§] Contact information for this author at Osaka City University. Phone: +81-6-6605-3149. Fax: +81-6-6605-3137.

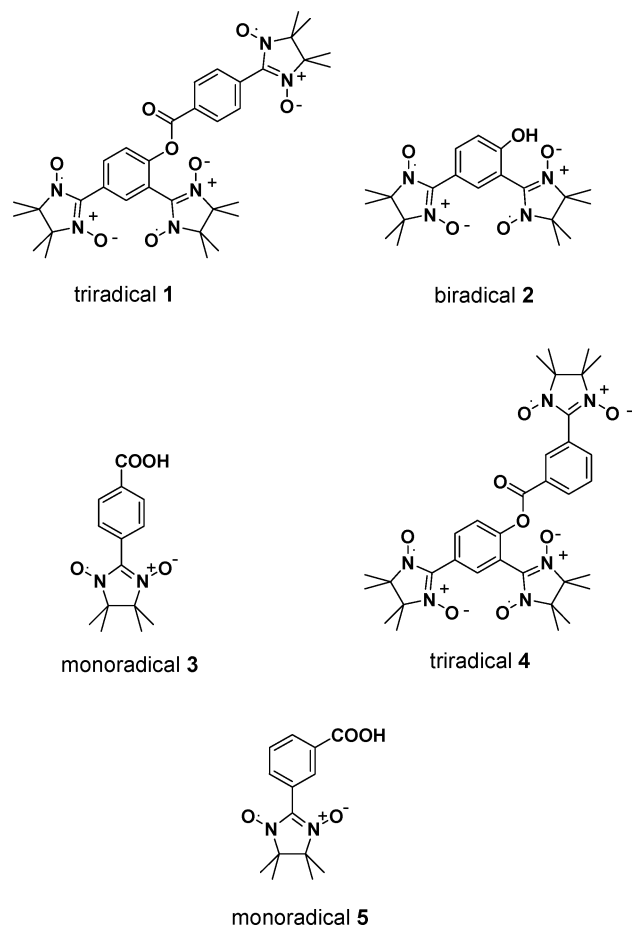


Figure 2. Triradicals **1** and **4** as building blocks for single-component ferrimagnetics and biradicals and monoradicals **2**, **3**, and **5** constituting the triradicals.

scheme, the requisite for the single-component approach is represented by

$$|J(\sigma)|, |J'(\sigma)| \ll J(\pi) \quad (2)$$

The eigenstates of the spin Hamiltonian eq 1 consist of one quartet ($S = 3/2$) state (abbreviated as “Q”) and two doublet ($S = 1/2$) states (“D1” and “D2”). The condition in eq 2 means that one of the two doublet states is quasidegenerate with Q and the other doublet state lies far apart above the quasidegenerate states. Intermolecular π -orbital overlaps between an $S = 1$ moiety of one molecule and an $S = 1/2$ moiety of the adjacent molecule mimic molecular complexation of π -biradicals and π -monoradicals, giving the possible ferrimagnetic spin alignment between the moieties with differing spins. This molecular designing features in the degree of freedom within the triradical molecule; the covalently united biradical and the monoradical moieties retain their magnetic degree of freedom of $S = 1$ and $1/2$, respectively, owing to the truncated π -conjugation.

In previous studies,^{8–10} we designed and synthesized a triradical **1** (Figure 2) from a phenol-substituted biradical **2** and a benzoic acid monoradical **3** as a building block of “single-component ferrimagnetics”. The phenol-based biradical **2** is known to have a triplet ($S = 1$) ground state with the singlet–triplet energy gap of $2J(\pi)/k_B = 26$ K,¹³ which is retained in the triradical **1** after the esterification with **3**.^{8,9,11} The amplitude of the additional interactions, $|J(\sigma)|$ and $|J'(\sigma)|$, of **1** has been estimated to be in the order of 100 mK from ^{14}N hyperfine splitting patterns of ESR spectra in a fluid solution^{8,9} and magnetic susceptibility measurements in the ultra-low-temper-

ature region down to 250 mK.⁸ The condition in eq 2 is realized for $J(\pi)$ larger than $|J(\sigma)|$ and $|J'(\sigma)|$ by 2 orders of magnitude in **1**. In the crystal of the triradical **1**, an alternating chain of the biradical and monoradical moieties has been established.⁸ The magnetic susceptibility of **1** shows a short-range ordering of $S = 1$ and $1/2$ spins along the alternating chain. Intrachain magnetic interactions, however, hindered a ferrimagnetic long-range ordering in the crystal of **1**.⁸

In this study, we have synthesized a positional isomer of **1**, the triradical **4**, in which a nitronyl nitroxide radical is substituted in the meta position in the monoradical moiety. The magnitude of the exchange couplings $J(\sigma)$ and $J'(\sigma)$ in **4** is expected to be outside the range for conventional magnetic susceptibility measurements, as found for the triradical **1**.^{8,9} We invoke hyperfine structures in solution-phase ESR spectra due to ^1H as well as ^{14}N nuclei to probe for traces of couplings $J(\sigma)$ and $J'(\sigma)$ in **4**. The analysis of the hyperfine structure appearing in ESR spectra of exchange-coupled systems can date back to pioneering work by Weissman,¹⁴ Luckhurst,¹⁵ and Rassat.¹⁶ The resonance field and intensity of hyperfine ESR transitions depend on the relative magnitudes of exchange interactions J and hyperfine coupling A . As described in the literature,^{14–18} the extreme limit of $|J| \gg |A|$ or $|J| \ll |A|$ gives simple hyperfine splitting patterns in ESR spectra reflecting the relative magnitude. In contrast, intermediate cases of $|J| \approx |A|$ give rise to complicated hyperfine splittings as compared with monoradicals of $S = 1/2$ with one unpaired electron. We present here an alternative approach based on perturbation treatments^{11,12} assuming that the amplitude of $J(\pi)$ is much larger than those of $|J(\sigma)|$ and $|J'(\sigma)|$. This approach gives an analytical form of resonance fields of hyperfine transitions due to ^{14}N and ^1H , and enables us to assign specific signals in complicated hyperfine splitting patterns, affording estimates for the magnitude of weak couplings $J(\sigma)$ and $J'(\sigma)$. Magnetic properties of **4** in the crystalline solid state are discussed on the basis of the X-ray crystal structure.

Experimental Section

The triradical **4** was synthesized by esterification of the phenol-based biradical **2**¹³ and the carboxylic acid monoradical **5**^{19,20} according to the method for the synthesis of the triradical **1**.^{8,9} Single crystals of **4** were obtained by recrystallization from acetone/cyclohexane solutions.

The X-ray diffraction measurements were made on a Rigaku Mercury CCD diffractometer at 233 K with graphite monochromated Mo K α radiation up to $2\theta_{\text{max}} = 55^\circ$. The crystal structure was solved by direct methods (SIR92)²¹ and succeeding Fourier syntheses followed by the full-matrix least-squares refinement with the anisotropic approximation for non-hydrogen atoms. Positions of the hydrogen atoms were calculated and included in the final refinement. All the calculations were made with the program package CrystalStructure by Rigaku/Molecular Structure Corporation.²²

The ESR spectra of **4** and **5** were recorded in toluene solutions, which were degassed by a freeze–pump–thaw cycle and sealed in vacuo, using a JEOL X-band spectrometer JES-FE2XG and a Bruker X-band spectrometer ESP300. The concentration of the solutions was 1×10^{-5} mol dm $^{-3}$.

The magnetic susceptibility was measured for randomly oriented polycrystalline samples of **4** on a Quantum Design SQUID Magnetometer MPMS-XL with an applied field of 0.1 T in the temperature range of 1.9–298 K.

Results and Discussion

1. DFT Molecular Orbitals and Phenomenological Spin Hamiltonian of Triradical 4. To obtain an estimate for the intramolecular exchange interactions through the σ -bonds, $J(\sigma)$ and $J'(\sigma)$, molecular orbitals (MOs) for the doublet ($S = 1/2$) and quartet ($S = 3/2$) states were calculated on the basis of the unrestricted density functional theory (DFT) by using the program package Gaussian98.²³ The molecular geometry was taken from an X-ray crystal structure as described below and the methyl groups were replaced by hydrogen atoms. At the SVWN/6-31+G(d,p) level,²⁴ the total electronic energy of the lowest doublet state is lower than the lowest quartet state by 7.7×10^{-7} hartree (2.1×10^{-5} eV, 0.24 K). The doublet state has positive spin densities on the ONCNO groups of the biradical moiety and negative in the monoradical moiety, whereas all three ONCNO groups have positive spin densities in the quartet state as expected.

The spin functions for the eigenstates of the Heisenberg spin Hamiltonian eq 1 are

$$\Psi(Q) = \frac{1}{\sqrt{3}}(\beta_{b1}\alpha_{b2}\alpha_m + \alpha_{b1}\beta_{b2}\alpha_m + \alpha_{b1}\alpha_{b2}\beta_m) \quad (3a)$$

$$\Psi(D1) = \frac{1}{\sqrt{2}}(\beta_{b1}\alpha_{b2}\alpha_m - \alpha_{b1}\beta_{b2}\alpha_m) \quad (3b)$$

$$\Psi(D2) = \frac{1}{\sqrt{2}}\left[\frac{1}{\sqrt{3}}(\beta_{b1}\alpha_{b2}\alpha_m + \alpha_{b1}\beta_{b2}\alpha_m) - \frac{2}{\sqrt{3}}\alpha_{b1}\alpha_{b2}\beta_m\right] \quad (3c)$$

for the limit of $J(\sigma)/J(\pi) \rightarrow 0$ and $J'(\sigma)/J(\pi) \rightarrow 0$,⁷ where α_n and β_n are the up- and down-spin functions of $S = 1/2$ at the site $n = b1, b2$, and m , respectively. The local spin polarization ρ for the three sites defined by

$$\rho \equiv \{\langle S_{b1}^z \rangle, \langle S_{b2}^z \rangle, \langle S_m^z \rangle\} \quad (4)$$

in the spin subspace with the z -component of $+1/2$ for the total spin was calculated from eq 3⁷ as

$$\rho(Q) = \{1/6, 1/6, 1/6\} \quad (5a)$$

$$\rho(D1) = \{0, 0, 1/2\} \quad (5b)$$

$$\rho(D2) = \{1/3, 1/3, -1/6\} \quad (5c)$$

The spin density distribution obtained by the DFT-based MO calculations indicates that the doublet and quartet states in the MO calculations correspond to the eigenstates Q (eqs 3a and 5a) and D2 (eqs 3c and 5c) of the phenomenological spin Hamiltonian eq 1, respectively. The energy separation between the states Q and D2 is given as

$$\Delta E(Q-D2) = -J(\pi) - J(\sigma) - J'(\sigma) + [J(\pi)^2 + J(\sigma)^2 + J'(\sigma)^2 - J(\pi)J(\sigma) - J(\pi)J'(\sigma) - J(\sigma)J'(\sigma)]^{1/2} \quad (6)$$

Approximation of $J(\sigma) \approx J'(\sigma)$ in eq 6 gives

$$\Delta E(Q-D2) \approx -3J(\sigma) \quad (7)$$

Thus, the total electronic energies from the DFT-based MO calculations give an estimate of $J(\sigma)/k_B \approx -0.24/3 = -0.08$ K. While the quantitative reliability of the quartet–doublet energy separation derived from the DFT-based MO calculations is not satisfactory, only the order of the $|J(\sigma)|/k_B$ value of 10^{-1}

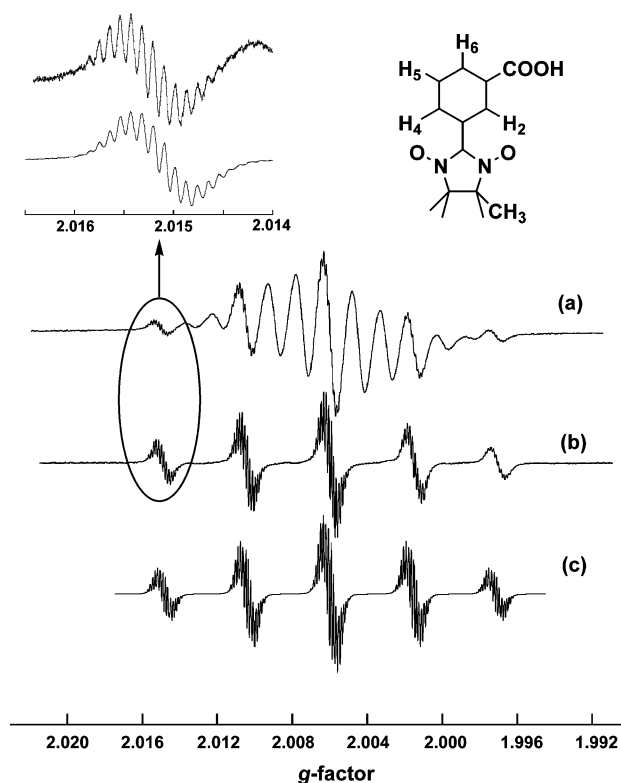


Figure 3. ESR spectra of the triradical **4** (a) and the monoradical **5** (b) in toluene solutions. The simulated spectrum of the monoradical **5** (c) is given by using the parameters $|A^N|/g\mu_B = 0.75$ mT, $|A^H(\text{methyl})|/g\mu_B = 0.021$ mT, $|A^H(2,4)|/g\mu_B = 0.051$ mT, $|A^H(5)|/g\mu_B = 0.021$ mT, $|A^H(6)|/g\mu_B = 0.042$ mT, the g -factor of $g = 2.006$, and the line width of $\Delta B = 0.0012$ mT. The abscissa is shown in the g -factor instead of the magnetic fields to facilitate the comparison of parts a and b, which have slight shifts to the center fields of hyperfine transitions due to a difference in the microwave frequencies: (a) 9.22491 and (b) 9.49266 GHz.

K is accepted. This is in the same order as that observed for the triradical **1**.^{8,9} The π -conjugation through the ester coupler is efficiently truncated in **4** as well as in **1**.

2. Solution ESR Spectra of Triradical 4. (a) *¹⁴N Hyperfine Structure.* The intramolecular exchange interactions between the three radical fragments $J(\pi)$, $J(\sigma)$, and $J'(\sigma)$ within the triradical molecule **4** were examined by ESR spectra in solutions. The ESR spectrum of **4** in a toluene solution is shown in Figure 3. The spectrum consists of 13 lines equally separated by 0.25 mT, which is about one-third of the hyperfine coupling constant for nitrogen nuclei of $I = 1$ in nitronyl nitroxide monoradicals.^{20,25} This spectral pattern indicates that hyperfine coupling constants A^N of six nitrogen nuclei in **4** are almost equivalent and that all the intramolecular exchange interactions $J(\pi)$, $J(\sigma)$, and $J'(\sigma)$ are larger than $|A^N|$. In our previous studies,^{9,11,12} the ¹⁴N hyperfine splitting patterns of nitronyl nitroxide triradicals have been analyzed by use of a spin Hamiltonian of eq 1 plus the electronic Zeeman and the ¹⁴N hyperfine terms

$$H = g\mu_B B(S_{b1}^z + S_{b2}^z + S_m^z) - 2J(\pi)S_{b1} \cdot S_{b2} - 2J(\sigma)S_{b1} \cdot S_m - 2J'(\sigma)S_{b2} \cdot S_m + A^N(I_{b1}^z S_{b1}^z + I_{b2}^z S_{b2}^z + I_m^z S_m^z) \quad (8)$$

$$I_n^z = I_n^z(1) + I_n^z(2) \quad (n = b1, b2, m) \quad (9)$$

where g , μ_B , and B stand for the g -factor, Bohr magneton, and the static magnetic field, respectively. The parameter A^N denotes

the isotropic hyperfine coupling constants of the ^{14}N nuclei for the biradical and monoradical moieties, where the difference in the coupling constants for the biradical and monoradical moieties is neglected. The spectral pattern of 13 lines with equal separations has appeared in the simulation based on eqs 8 and 9 in a strong-exchange limit of $|J(\pi)|$, $|J(\sigma)|$, $|J'(\sigma)| > 10 \times |A^{\text{N}}|$.^{9,11,12} It has been known that the simulated hyperfine splitting patterns are insensitive to the difference of $|J(\pi)|$, $|J(\sigma)|$, and $|J'(\sigma)|$ in the strong exchange limit.^{9,11,12} Although the amplitude of $J(\pi)$ is expected to be much larger than those of $J(\sigma)$ and $J'(\sigma)$ from the chemical structure of **4**, the deviation of molecular symmetry of exchange interactions from equilateral as well as isosceles triangles is not detectable in hyperfine ESR spectroscopy of fluid solutions for the strong exchange limit. The observed ESR spectrum gives us only the lower limit of the amplitude of exchange interactions in the triradical **4**; $|J(\pi)|$, $|J(\sigma)|$, $|J'(\sigma)| > 10 \times |A^{\text{N}}|$, i.e., $|J(\pi)|/k_{\text{B}}$, $|J(\sigma)|/k_{\text{B}}$, $|J'(\sigma)|/k_{\text{B}} > 10$ mK for $|A^{\text{N}}|/g\mu_{\text{B}} \sim 0.75$ mT and $g = 2.0$.

(b) ^1H Hyperfine Structure. As found in the observed spectrum of **4** in Figure 3, additional splittings are superposed on the 1st, 4th, 7th, 10th, and 13th lines of the ^{14}N hyperfine splitting. The superposed splittings in **4** (Figure 3a) coincide with the ^1H hyperfine structure of a *m*-benzoic acid derivative of monoradical **5** (Figure 3b). The observed spectrum of the monoradical **5** was reproduced by the simulation with the hyperfine coupling constants $|A^{\text{N}}|/g\mu_{\text{B}} = 0.75$ mT, $|A^{\text{H}}(\text{methyl})|/g\mu_{\text{B}} = 0.021$ mT, $|A^{\text{H}}(2,4)|/g\mu_{\text{B}} = 0.051$ mT, $|A^{\text{H}}(5)|/g\mu_{\text{B}} = 0.021$ mT, $|A^{\text{H}}(6)|/g\mu_{\text{B}} = 0.042$ mT, the g -factor of $g = 2.006$, and the line width of $\Delta B = 0.0012$ mT for the Lorentzian lines. The hyperfine coupling constants for **5** are in agreement with those for nitronyl nitroxide monoradicals with similar structures.²⁵ Thus, both ^{14}N and ^1H hyperfine splittings attributable to a meta-substituted nitronyl nitroxide monoradical are superposed to the spectrum of the triradical **4**.

The superposition found in the spectrum of **4** was analyzed in terms of a spin Hamiltonian including both the ^{14}N and ^1H hyperfine coupling terms. This gives the relative amplitude of $|J(\pi)|$, $|J(\sigma)|$, and $|J'(\sigma)|$, which has been missed in the hyperfine structure analysis of only ^{14}N nuclei. We have reported an ESR spectral analysis of nitroxide-based triradicals on the basis of perturbation treatments^{11,12} assuming that the exchange interaction within the biradical moiety $J(\pi)$ is much larger than those between the biradical and monoradical moieties $|J(\sigma)|$ and $|J'(\sigma)|$. This approach is applied to the explanation of the superposition by introducing the ^1H hyperfine coupling terms as well as those of ^{14}N . To the spin Hamiltonian eq 8 is added the ^1H hyperfine coupling terms and it is split into two parts, $H^{(0)}$ and $H^{(1)}$, or $H^{(0)}$ and $H^{(2)}$:

$$H = H^{(0)} + H^{(1)} \quad (10a)$$

$$H^{(0)} = g\mu_{\text{B}}B(S_{\text{b1}}^z + S_{\text{b2}}^z + S_{\text{m}}^z) - 2J(\pi)\mathbf{S}_{\text{b1}} \cdot \mathbf{S}_{\text{b2}} \quad (10b)$$

$$H^{(1)} = -2J(\sigma)\mathbf{S}_{\text{b1}} \cdot \mathbf{S}_{\text{m}} - 2J'(\sigma)\mathbf{S}_{\text{b2}} \cdot \mathbf{S}_{\text{m}} + A_{\text{b1}}I_{\text{b1}}^z S_{\text{b1}}^z + A_{\text{b2}}I_{\text{b2}}^z S_{\text{b2}}^z + A_{\text{m}}I_{\text{m}}^z S_{\text{m}}^z \quad (10c)$$

$$H = H^{(0)} + H^{(2)} \quad (10d)$$

$$H^{(2)} = -2J(\sigma)\mathbf{S}_{\text{b1}} \cdot \mathbf{S}_{\text{m}} - 2J'(\sigma)\mathbf{S}_{\text{b2}} \cdot \mathbf{S}_{\text{m}} + (A_{\text{b1}}^1 I_{\text{b1}}^z + A_{\text{b1}}^2 I_{\text{b1}}^z) S_{\text{b1}}^z + (A_{\text{b2}}^1 I_{\text{b2}}^z + A_{\text{b2}}^2 I_{\text{b2}}^z) S_{\text{b2}}^z + (A_{\text{m}}^1 I_{\text{m}}^z + A_{\text{m}}^2 I_{\text{m}}^z) S_{\text{m}}^z \quad (10e)$$

The unperturbed Hamiltonian $H^{(0)}$ consists of the electronic Zeeman interaction and the Heisenberg exchange interaction $J(\pi)$ through the π -conjugation in the *m*-phenylene moiety of the biradical. The perturbation Hamiltonian $H^{(1)}$ or $H^{(2)}$ is

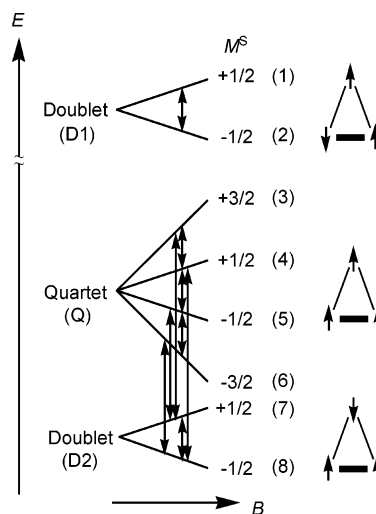


Figure 4. Energy diagram for the triradicals **1** and **4**. The Zeeman sublevels are designated by the quantum numbers M^{S} of the total spin and the numbers in parentheses, which correspond to those listed in Table 1. The arrows connecting the Zeeman sublevels indicate the allowed ESR transitions. The hyperfine sublevels are omitted for clarity. In the right side are shown the schematic representations of electron spin configurations for the quartet (Q) and doublet (D1, D2) states.

composed of the exchange interactions between the biradical and monoradical moieties and the hyperfine couplings. The Hamiltonian $H^{(1)}$ or $H^{(2)}$ includes one or two kinds of inequivalent nuclear spins, respectively, existing in each of the radical fragment of the monoradical and the biradical moieties. The two nuclei and their coupling constants are designated by the superscripts A^1 , I^1 and A^2 , I^2 in $H^{(2)}$. The spin Hamiltonian eq 10 is represented by a $2^3 \times 2^3$ matrix, which is set up in the ket space spanned by the basis kets for the quantum numbers of electron spins m^{S} and nuclear spins m^{I}

$$S_n^z |m_{\text{b1}}^{\text{S}}, m_{\text{b2}}^{\text{S}}, m_{\text{m}}^{\text{S}}, m^{\text{I}}\rangle = m_n^{\text{S}} |m_{\text{b1}}^{\text{S}}, m_{\text{b2}}^{\text{S}}, m_{\text{m}}^{\text{S}}, m^{\text{I}}\rangle \quad (\text{n} = \text{b1}, \text{b2}, \text{m}) \quad (11a)$$

$$M^{\text{S}} = m_{\text{b1}}^{\text{S}} + m_{\text{b2}}^{\text{S}} + m_{\text{m}}^{\text{S}} \quad (11b)$$

The nuclear quantum number m^{I} is the collective index for a spin configuration

$$m^{\text{I}} = \{m_{\text{b1}}, m_{\text{b2}}, m_{\text{m}}\} \quad (12a)$$

for eq 10c or

$$m^{\text{I}} = \{m_{\text{b1}}^1, m_{\text{b2}}^1, m_{\text{m}}^1, m_{\text{b1}}^2, m_{\text{b2}}^2, m_{\text{m}}^2\} \quad (12b)$$

for eq 10e. As we have reported in previous papers,^{11,12} the matrix for $H^{(0)}$ can be exactly diagonalized and the perturbed energy $E(i)$ of the i th spin state can be calculated analytically to the first order.

The spin Hamiltonian eq 10, as well as eq 1, affords one quartet (Q) and two doublet states (D1, D2) with respect to the electron spins, which are depicted in Figure 4. We have 15 allowed transitions with $\Delta M^{\text{S}} = \pm 1$, i.e., 15 pairs of spin states (5 within the multiplets and 10 across the multiplets) in the three-spin system for one set of the nuclear spin configuration, eq 12a or eq 12b. When the exchange coupling within the biradical moiety $J(\pi)$ is much larger than all other exchange interactions, as expected for the triradical **4**, one of the two doublet states D1 lies far apart above the other doublet (D2) and the quartet (Q) states. Therefore, we neglect the contribution

TABLE 1: First-Order Resonance Fields $\delta\Delta E(i \leftrightarrow j) = g\mu_B\{B_0 - B(i \leftrightarrow j)\}$ (B_0 is the center field) of Allowed ESR Transitions Derived from the Spin Hamiltonian Eq 10a and Eq 10d

$i-j$	multiplet	$\delta\Delta E(i \leftrightarrow j)^a$ (eq 10a)	$\delta\Delta E(i \leftrightarrow j)$ (eq 10d)
1–2	D1–D1	$A_m m_m$	$A_m^1 m_m^1 + A_m^2 m_m^2$
3–4	Q–Q	$1/4[-3J(\sigma) - 3J'(\sigma) + A_{b1}m_{b1} + A_{b2}m_{b2} + 2A_m m_m + E_{34}]$	b
4–5	Q–Q	$1/4[2(A_{b1}m_{b1} + A_{b2}m_{b2}) - E_{34} + E_{67}]$	b
5–6	Q–Q	$1/4[3J(\sigma) + 3J'(\sigma) + A_{b1}m_{b1} + A_{b2}m_{b2} + 2A_m m_m - E_{67}]$	b
7–8	D2–D2	$1/4[2(A_{b1}m_{b1} + A_{b2}m_{b2}) + E_{34} - E_{67}]$	b
3–7	Q–D2	$1/4[-3J(\sigma) - 3J'(\sigma) + A_{b1}m_{b1} + A_{b2}m_{b2} + 2A_m m_m - E_{67}]$	b
4–8	Q–D2	$1/4[2(A_{b1}m_{b1} + A_{b2}m_{b2}) - E_{34} - E_{67}]$	b
5–7	Q–D2	$1/4[2(A_{b1}m_{b1} + A_{b2}m_{b2}) + E_{34} + E_{67}]$	b
6–8	Q–D2	$1/4[3J(\sigma) + 3J'(\sigma) + A_{b1}m_{b1} + A_{b2}m_{b2} + 2A_m m_m + E_{67}]$	b

^a $E_{34} = [8(J(\sigma) + J'(\sigma))^2 + (J(\sigma) + J'(\sigma) + A_{b1}m_{b1} + A_{b2}m_{b2})^2 - 4A_m m_m(J(\sigma) + J'(\sigma) + A_{b1}m_{b1} + A_{b2}m_{b2}) + 4(A_m m_m)^2]^{1/2}$. $E_{67} = [8(J(\sigma) + J'(\sigma))^2 + (J(\sigma) + J'(\sigma) - A_{b1}m_{b1} - A_{b2}m_{b2})^2 + 4A_m m_m(J(\sigma) + J'(\sigma) - A_{b1}m_{b1} - A_{b2}m_{b2}) + 4(A_m m_m)^2]^{1/2}$. b Complicated function of $J(\sigma)$, $J'(\sigma)$, A_n^1 , A_n^2 , m_n^1 , and m_n^2 ($n = b1, b2, m$).

from allowed ESR transitions across the multiplets, i.e., those between D1 and Q or D1 and D2. We have only nine pairs of states, five within the multiplets and four across the multiplets of Q and D2. The transition energies for the nine allowed transitions were calculated to the first order from the perturbed energies $E(i)$

$$\Delta E(i \leftrightarrow j) \equiv E(i) - E(j) = h\nu \quad (13)$$

$$\delta\Delta E(i \leftrightarrow j) \equiv \Delta E(i \leftrightarrow j) - g\mu_B B \quad (14)$$

where ν stands for the microwave frequency. The transition fields $\delta\Delta E(i \leftrightarrow j)/g\mu_B$ as measured from the center field B_0

$$B(i \leftrightarrow j) = B_0 - \delta\Delta E(i \leftrightarrow j)/g\mu_B \quad (15)$$

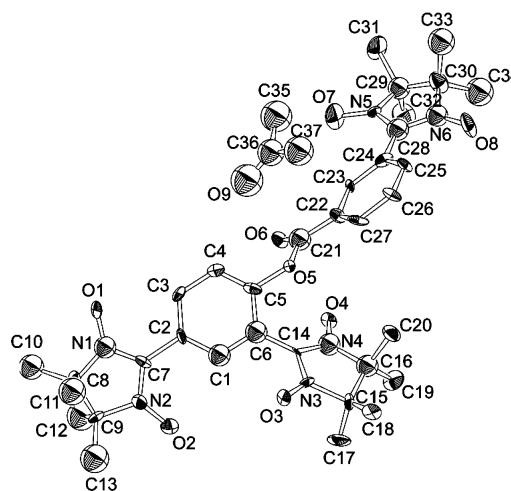
$$B_0 \equiv h\nu/g\mu_B \quad (16)$$

are listed in Table 1 for both eqs 10a and 10d. We found from the calculated results for eq 10a, i.e., the system for one nucleus per fragment, that the resonance field $\delta\Delta E(1 \leftrightarrow 2)/g\mu_B$ is independent of $J(\sigma)$ and $J'(\sigma)$ and is a function of the hyperfine coupling constant A_m and the nuclear spin quantum number m_m of the monoradical moiety. This resonance field is independent of A_{b1} , A_{b2} , m_{b1} , and m_{b2} of the biradical moiety. The resonance fields of all the transitions except $\Delta E(1 \leftrightarrow 2)$ depend on $J(\sigma)$, $J'(\sigma)$, and the nuclear spin quantum numbers m_{b1} and m_{b2} . The perturbation calculations tell us that allowed ESR transitions appear which exhibit hyperfine splitting only of the monoradical moiety under the condition of $J(\pi) \gg |J(\sigma)|$, $|J'(\sigma)|$ (eq 2). This occurs independently of the number of inequivalent nuclei: The resonance field $\delta\Delta E(1 \leftrightarrow 2)/g\mu_B$ derived from eq 10d, which contains two inequivalent nuclei, e.g., ^{14}N and ^1H , is independent of the biradical-related coupling constants and quantum numbers $J(\sigma)$, $J'(\sigma)$, A_{b1} , A_{b2} , m_{b1} , and m_{b2} . The superposition of the ^1H hyperfine splittings on the 1st, 4th, 7th, 10th, and 13th signals of the ^{14}N hyperfine splitting in the observed ESR spectra of the triradical **4** is assigned to the transition $\Delta E(1 \leftrightarrow 2)$ in D1. Resonance fields of other transitions have a contribution from $J(\sigma)$ and $J'(\sigma)$. The amplitude of these interactions should fluctuate owing to conformational interconversion of the molecule **4** in solutions. The fluctuation results in a broadening of the signals except $\Delta E(1 \leftrightarrow 2)$. The broadening, or the seeming reduction in intensity, for the signals except for $\Delta E(1 \leftrightarrow 2)$ is responsible for the absence of the ^1H hyperfine splittings on the 2nd, 3rd, 5th, 6th, ... of the ^{14}N hyperfine transitions. The appearance of the superposition indicates that the exchange interactions $J(\sigma)$ and $J'(\sigma)$ are very small as compared with $J(\pi)$ in **4**. The analyses of the ^{14}N and ^1H hyperfine splittings based

TABLE 2: Crystallographic Data for 4

formula	$\text{C}_{34}\text{H}_{43}\text{N}_6\text{O}_8 \cdot \text{C}_3\text{H}_6\text{O}$
formula wt	721.83
crystal system	orthorhombic
space group	$Pca2_1$ (no. 29)
$a/\text{\AA}$	14.770(7)
$b/\text{\AA}$	20.689(9)
$c/\text{\AA}$	12.699(5)
$V/\text{\AA}^3$	3880(2)
Z	4
$D_{\text{calc}}/\text{g cm}^{-3}$	1.235
T/K	233
no. of reflcns measd	7334
no. of unique reflcns used ($I > 1.5\sigma(I)$)	4392
R, R_w^a	0.123, 0.210

^a The function minimized is $\sum w(|F_o| - |F_c|)^2$, where $w = 1/[0.0293F_o^2 + \sigma(F_o^2)]$. The residuals are defined as $R = \sum ||F_o| - |F_c||/\sum |F_o|$, $R_w = (\sum w(|F_o| - |F_c|)^2/\sum wF_o^2)^{1/2}$.

**Figure 5.** ORTEP drawing of **4** with thermal ellipsoids of 50% probability.

on the perturbation calculations lead to the conclusion of the relative amplitude of the exchange and hyperfine coupling constants:

$$|A^N| \ll |J(\sigma)|, |J'(\sigma)| \ll J(\pi) \quad (17)$$

3. Crystal Structure of Triradical 4. The crystallographic data for the triradical **4** are summarized in Table 2. The crystal contains 1 mol of acetone as crystal solvent. An ORTEP drawing of the molecule is depicted in Figure 5. The thermal parameters for carbon and oxygen atoms of acetone are quite large,

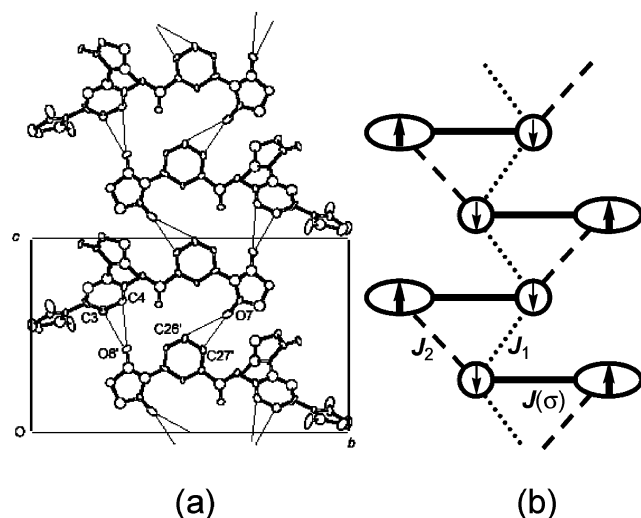


Figure 6. (a) Molecular chain of **4** along the *c*-axis. The neighboring molecules are related by the 2-fold screw axis along the *c*-axis. The thin solid lines represent the intermolecular short contacts (C3–O8': 3.20(1) Å; C4–O8': 3.46(1) Å; O7–C26': 3.41(1) Å; O7–C27': 3.07(1) Å). (b) Schematic diagram for the chain. The circles and the ovals show the monoradical and the biradical moieties, respectively. The dotted and dashed lines represent the intermolecular exchange interactions J_1 and J_2 , while the thick solid line denotes the intramolecular interaction $J(\sigma)$ or $J'(\sigma)$. The arrows indicate the spin alignment at low temperature.

reflecting a positional disorder. Carbon atoms of the methyl groups in nitronyl nitroxide of the triradical **4** have large thermal parameters as well. The disorder results in an *R*-factor larger than 0.1.²⁶ Figure 6a shows the crystal structure projected onto the *bc* plane. Nearest-neighbor molecules related by the 2-fold screw axis are arranged along the *c*-axis. Intermolecular short contacts *d* are found between the oxygen atoms of nitronyl nitroxide and the carbon atoms of the phenyl rings in the molecules neighboring along the *c*-axis: Between the nitroxide group of the monoradical moiety and the phenyl ring of the biradical moiety are found two contacts at $d(\text{C3}–\text{O8}') = 3.20(1)$ Å and $d(\text{C4}–\text{O8}') = 3.46(1)$ Å, whereas contacts at $d(\text{O7}–\text{C26}') = 3.41(1)$ Å and $d(\text{O7}–\text{C27}') = 3.07(1)$ Å are found between the nitroxide group and the phenyl ring of the monoradical moieties. These short contacts lead to a molecular chain along the *c*-axis, which is schematically shown in Figure 6b. The short contacts at O7 and O8 should give intermolecular exchange interactions, as designated by J_1 and J_2 in Figure 6b. These intermolecular interactions, together with the intramolecular interactions, $J(\sigma)$ and $J'(\sigma)$, afford a structured chain of $S = 1/2$ and 1 spins, as depicted in Figure 6b.

4. Magnetic Susceptibility of Triradical 4. Figure 7 shows the temperature dependence of paramagnetic susceptibility χ_p measured for a randomly oriented polycrystalline sample of **4**. The $\chi_p T$ value is 1.132 emu K mol^{−1} at room temperature. This is in good agreement with the expected value of three uncorrelated (noninteracting) $S = 1/2$ spins with the *g*-factor of 2.006, which was observed in the ESR spectra. With decreasing temperature the $\chi_p T$ value increased to reach the maximum of 1.21 emu K mol^{−1} at 13 K. Below this temperature, the $\chi_p T$ value decreased down to 0.77 emu K mol^{−1} at the base temperature of 1.9 K. The increase in $\chi_p T$ indicates that the dominating exchange interaction in the crystalline solid of **4** is ferromagnetic, which is assigned to $J(\pi)$ within the molecule. The decrease in $\chi_p T$ at low temperature tells us that additional

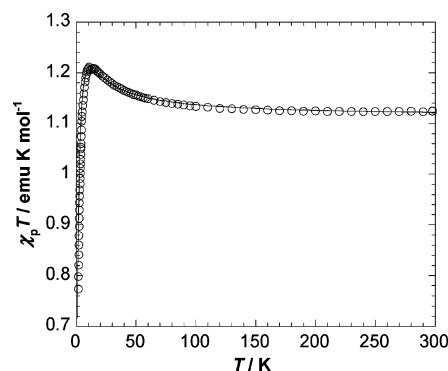


Figure 7. Temperature dependence of magnetic susceptibility χ_p of **1** measured on a SQUID magnetometer with *B* = 0.1 T in the $\chi_p T$ vs *T* plot. The solid line denotes the calculated values from eq 18 ($J(\pi)/k_B = 9.5$ K, $\theta = -0.9$ K).

weak antiferromagnetic interactions occur. The temperature dependence of $\chi_p T$ is analyzed by using the equation

$$\chi_p = \frac{2N_A g^2 \mu_B^2}{3k_B(T - \theta)} \times \frac{3}{3 + \exp(-2J(\pi)/k_B T)} + \frac{N_A g^2 \mu_B^2}{3k_B(T - \theta)} \times \frac{3}{4} \quad (18)$$

In eq 18, the first term represents the singlet–triplet equilibrium of the biradical moiety with the singlet–triplet energy gap of $2J(\pi)$, in which two of the three $S = 1/2$ spins participate. The remaining $S = 1/2$ spin is assumed to obey the Curie–Weiss law as represented by the second term. This model assumes that the exchange interactions $J(\sigma)$, $J'(\sigma)$, J_1 , and J_2 are much smaller than $J(\pi)$ ²⁷ and they are collectively approximated by the mean field θ , which is set to be common in the first and the second terms. The fit to the observed temperature dependence of $\chi_p T$ gave the parameters $J(\pi)/k_B = 9.5 \pm 0.2$ K and $\theta = -0.9 \pm 0.1$ K. The *g*-factor was fixed as *g* = 2.006. The amplitude of the intramolecular ferromagnetic interaction $J(\pi)$ in the biradical moiety is close to those of triradicals with similar molecular structures of the *m*-phenylene-bis(nitronyl nitroxide) moiety.^{9,11} The mean-field θ is regarded as an average of $J(\sigma)$, $J'(\sigma)$, J_1 , and J_2 .

One-dimensional ferrimagnetic spin chains are known to exhibit a minimum and upturn of $\chi_p T$ on lowering the temperature.⁵ No such ferrimagnetic behavior of $\chi_p T$ was found for **4** in the temperature range examined. If the exchange interactions $J(\sigma)$, $J'(\sigma)$, and J_2 have negative signs suitable for an antiferromagnetic spin alignment of $S = 1$ and $1/2$, a ferrimagnetic spin alignment is expected along the molecular chain below our base temperature of 1.9 K, as depicted in Figure 7b. The other intermolecular interaction J_1 is favored by the ferrimagnetic spin alignment if it is ferromagnetic. Magnetic susceptibility measurements at ultralow temperature (<1.9 K) are underway.

Conclusion

As a model building block for the single-component molecule-based ferrimagnetics, the nitronyl nitroxide triradical **4** has been synthesized, in which a ground-state triplet biradical and a monoradical are covalently united. The ESR spectra from **4** in solutions exhibited 13 lines of hyperfine splitting attributable to six ¹⁴N nuclei of *I* = 1. A significant feature in the ESR spectra is the ¹H hyperfine splitting superposed in every third line of the ¹⁴N splittings. The appearance of the superposed hyperfine structure is rationalized by the perturbation calcula-

tions of the spin Hamiltonian assuming that the exchange interaction $J(\pi)$ in the π -conjugation of the biradical moiety is much larger than those between the biradical and the monoradical moieties $J(\sigma)$ and $J'(\sigma)$. This result indicates that the magnetic degree of freedom for $S = 1$ and $1/2$ is retained in **4**: The biradical with an $S = 1$ spin and the monoradical with an $S = 1/2$ spin are united in chemical terms, but they are kept independent in magnetic terms.

It has been found from the X-ray crystal structure analysis that the biradical and monoradical moieties are packed in a one-dimension chain in the crystal. The magnetic susceptibility of **4** indicates that the intermolecular exchange interactions along the chain are in the same order of magnitude as $J(\sigma)$ and $J'(\sigma)$, which are elaborately minimized by molecular designing of the single-component approach. The approach yields cocrystallization for two distinct molecules having differing spins with ultimate reliability. Ferrimagnetic behavior for **4**, however, has not been found in the temperature range examined, which is ascribed to the weak intermolecular interactions. A more precise control on molecular packing, or crystal engineering, is necessary for obtaining genuinely organic molecule-based ferromagnets.

Acknowledgment. This work has been supported by Grants-in-Aid for Scientific Research from the Ministry of Education, Sports, Culture, Science and Technology, Japan. Financial support from PRESTO of Japan Science and Technology Agency (JST) is also acknowledged. The authors thank Professor Nobuyuki Aikawa at Osaka City University for help in the X-ray diffraction experiments.

Supporting Information Available: Crystallographic data (CIF file) and a table of atomic spin densities calculated by the DFT methods. This material is available free of charge via the Internet at <http://pubs.acs.org>.

References and Notes

- (1) For recent overviews of molecule-based magnetism, see: (a) Christou, G., Ed. *Polyhedron* **2003**, *22*. (b) Christou, G., Ed. *Polyhedron* **2001**, *20*. (c) Itoh, K.; Kinoshita, M., Eds. *Molecular Magnetism*; Gordon and Breach: Amsterdam, The Netherlands (Kodansha: Tokyo, Japan), 2000. (d) Lahti, P. M., Ed. *Magnetic Properties of Organic Materials*; Marcel Dekker: New York, 1999.
- (2) (a) Tamura, M.; Nakazawa, Y.; Shiomi, D.; Nozawa, K.; Hosokoshi, Y.; Ishikawa, M.; Takahashi, M.; Kinoshita, M. *Chem. Phys. Lett.* **1991**, *186*, 401. (b) Nakazawa, Y.; Tamura, M.; Shirakawa, N.; Shiomi, D.; Takahashi, M.; Kinoshita, M.; Ishikawa, M. *Phys. Rev. B* **1992**, *46*, 8906.
- (3) (a) Izuoka, A.; Fukada, M.; Kumai, R.; Itakura, M.; Hikami, S.; Sugawara, T. *J. Am. Chem. Soc.* **1994**, *116*, 2609. (b) Shiomi, D.; Nishizawa, M.; Sato, K.; Takui, T.; Itoh, K.; Sakurai, H.; Izuoka, A.; Sugawara, T. *J. Phys. Chem. B* **1997**, *101*, 3342. (c) Nishizawa, M.; Shiomi, D.; Sato, K.; Takui, T.; Itoh, K.; Sawa, H.; Kato, R.; Sakurai, H.; Izuoka, A.; Sugawara, T. *J. Phys. Chem. B* **2000**, *104*, 503.
- (4) Buchachenko, A. L. *Dokl. Akad. Nauk. Engl. Ed.* **1979**, *244*, 107.

- (5) Shiomi, D.; Sato, K.; Takui, T. *J. Phys. Chem. B* **2000**, *104*, 1961.
- (6) Shiomi, D.; Sato, K.; Takui, T. *J. Phys. Chem. B* **2001**, *105*, 2932.
- (7) Shiomi, D.; Sato, K.; Takui, T. *J. Phys. Chem. A* **2002**, *106*, 2096.
- (8) Shiomi, D.; Kanaya, T.; Sato, K.; Mito, M.; Takeda, K.; Takui, T. *J. Am. Chem. Soc.* **2001**, *123*, 11823.
- (9) Kanaya, T.; Shiomi, D.; Sato, K.; Takui, T. *Polyhedron* **2001**, *20*, 1397.
- (10) Shiomi, D.; Nishizawa, M.; Kamiyama, K.; Hase, S.; Kanaya, T.; Sato, K.; Takui, T. *Synth. Met.* **2001**, *121*, 1810.
- (11) Kaneda, C.; Shiomi, D.; Sato, K.; Takui, T. *Polyhedron* **2003**, *22*, 1809.
- (12) Shiomi, D.; Kaneda, C.; Kanaya, T.; Sato, K.; Takui, T. *Appl. Magn. Reson.* **2003**, *23*, 495.
- (13) Hase, S.; Shiomi, D.; Sato, K.; Takui, T. *J. Mater. Chem.* **2001**, *11*, 756.
- (14) Reitz, D. C.; Weissman, S. I. *J. Chem. Phys.* **1960**, *33*, 700.
- (15) Luckhurst, G. R. *Mol. Phys.* **1966**, *10*, 543.
- (16) (a) Dupeyre, R. M.; Lemaire, H.; Rassat, A. *J. Am. Chem. Soc.* **1965**, *87*, 3771. (b) Briere, R.; Dupeyre, R. M.; Lemaire, H.; Morat, C.; Rassat, A.; Rey, P. *Bull. Soc. Chim. France* **1965**, 3290.
- (17) Nakajima, A.; Ohya-Nishiguchi, H.; Deguchi, Y. *Bull. Chem. Soc. Jpn.* **1972**, *45*, 713.
- (18) Luckhurst, G. R.; Pedulli, G. F. *J. Am. Chem. Soc.* **1970**, *92*, 4738.
- (19) Schatzschneider, U.; Weyhermueller, T.; Rentschler, E. *Inorg. Chim. Acta* **2002**, *337*, 122.
- (20) Ullman, E. F.; Osiecki, J. H.; Boocock, D. G. B.; Darcy, R. J. *J. Am. Chem. Soc.* **1972**, *94*, 7049.
- (21) Altomare, A.; Burla, M. C.; Camalli, M.; Cascarano, M.; Giacovazzo, C.; Guagliardi, A.; Polidre, G. *J. Appl. Crystallogr.* **1994**, *27*, 435.
- (22) (a) *CrystalStructure*, ver.3.6.0; Rigaku and Rigaku/MS (2000–2004); 9009 New Trails Dr., The Woodlands, TX 77381. (b) *CRYSTALS*, issue 10; Watkin, D. J., Prout, C. K., Carruthers, J. R., Betteridge, P. W.; Chemical Crystallography Laboratory: Oxford, UK, 1996.
- (23) Frisch, M. J.; Trucks, G. W.; Schlegel, H. B.; Scuseria, G. E.; Robb, M. A.; Cheeseman, J. R.; Zakrzewski, V. G.; Montgomery, J. A., Jr.; Stratmann, R. E.; Burant, J. C.; Dapprich, S.; Millam, J. M.; Daniels, A. D.; Kudin, K. N.; Strain, M. C.; Farkas, O.; Tomasi, J.; Barone, V.; Cossi, M.; Cammi, R.; Mennucci, B.; Pomelli, C.; Adamo, C.; Clifford, S.; Ochterski, J.; Petersson, G. A.; Ayala, P. Y.; Cui, Q.; Morokuma, K.; Malick, D. K.; Rabuck, A. D.; Raghavachari, K.; Foresman, J. B.; Cioslowski, J.; Ortiz, J. V.; Stefanov, B. B.; Liu, G.; Liashenko, A.; Piskorz, P.; Komaromi, I.; Gomperts, R.; Martin, R. L.; Fox, D. J.; Keith, T.; Al-Laham, M. A.; Peng, C. Y.; Nanayakkara, A.; Gonzalez, C.; Challacombe, M.; Gill, P. M. W.; Johnson, B. G.; Chen, W.; Wong, M. W.; Andres, J. L.; Head-Gordon, M.; Replogle, E. S.; Pople, J. A. *Gaussian 98*, Revision A.9; Gaussian, Inc., Pittsburgh, PA, 1998.
- (24) The expectation values $\langle S^2 \rangle$ for the doublet ground state are 1.7694 and 0.8158 before and after the spin-projection, i.e., the annihilation of higher spin multiplicity components, respectively, while those for the quartet state are 3.7694 and 3.7502. The energy preference of stability for the doublet compared to the quartet state was found in calculations with other functionals such as B3LYP and other basis sets as well. The spin contamination for the doublet state was least for SVWN/6-31+G(d, p).
- (25) Cirujeda, J.; Vidal-Gancedo, J.; Jürgens, O.; Mota, F.; Novoa, J. J.; Rovira, C.; Veciana, J. *J. Am. Chem. Soc.* **2000**, *122*, 11393.
- (26) On the final difference Fourier map, density peaks were found around the acetone molecule and the methyl groups of **4**. The refinement of the disordered atoms of oxygen and carbon was unsuccessful, resulting in divergence of the least-squares calculation.
- (27) The amplitude of the interactions $J(\pi)$, $J(\sigma)$, and $J'(\sigma)$ of **4** in a fluid solution is possibly altered when the molecules are embedded in a crystal lattice. It is assumed that the relative orders of magnitude for the interactions, eq 17, determined from ESR spectroscopy in fluid solutions remain unchanged.